Rönnow *et al. Journal of Wood Science* (2022) 68:22
https://doi.org/10.1186/s10086-022-02026-5

Journal of Wood Science

ORIGINAL ARTICLE Open Access

Microwave complex permittivity and anisotropy of conifer wood chips vs moisture content: experiments and modeling

D. Rönnow[1*], P. Ottosson[2] and D. Andersson[2]

Abstract

The complex microwave permittivity—including anisotropy- of wood chips of softwood has been measured for different moisture contents in the band 0.75 to 2.5 GHz using an ultra-wide band radio transmission technique. The real and imaginary parts increase monotonically with moisture content. The wood chips are oriented by gravity, which gives anisotropic permittivity. The anisotropy ratio of the real part increases from 1.1 to 1.6 with moisture content from 0 to 120%. The anisotropy ratio of the imaginary part is around 2.5 at all moisture contents. Effective medium models were used to model the permittivity. The Bruggeman, and two versions of the Maxwell Garnett model gave good results at low moisture content (below the fiber saturation point). Above the fiber saturation point only the Bruggeman model gave results in agreement with experiments. The difference in model performance suggests that the free water does not follow the wood chips geometry.

Keywords: Permittivity, Moisture content, Anisotropy, Effective medium modeling, Wood chips, Soft wood, Ultra wideband radar

Introduction

Wood chips are used in pulp and paper industry and as fuel in district heating. The moisture content of wood chips influences the combustion and emission of carbon dioxide [1, 2] and has been found to be an important quality parameter in process control in pulp mills [3]. It may also change during storage [4]. To measure the moisture content has therefore attracted interest and indirect methods like near-infrared spectroscopy, X-ray absorption, and radio frequency and microwave methods are used [5, 6].

The microwave permittivity of wood chips changes significantly with moisture content [7, 8]. The measured complex permittivity of sawdust in the range 0.5 to 15 GHz was reported in [7] and varied with moisture. Ottosson et al. [8] determined the permittivity (real part) of wood chips in volumes of several m^3 using ultra wideband (UWB) radar; the permittivity was found to be anisotropic, which was caused by the orientation of the woodchips by gravity, and the anisotropy increased with increasing moisture content.

Effective medium models or mixing models are used to calculate an effective dielectric permittivity of inhomogeneous composite materials [9, 10]. The permittivity of the constituent materials as well as their volume fractions are used in the models. There are numerous effective medium models and if a specific model is suitable for a specific composite depends on various parameters, such as the geometry, volume fractions and permittivity of the constituents.

Paz et al. [11] measured the permittivity of woody biomass at 0.3–0.8 GHz and found that the Maxwell Garnett effective medium model was suitable for modeling the real part of permittivity vs moisture content. The

*Correspondence: daniel.ronnow@hig.se
[1] Department of Electrical Engineering, Mathematics and Science, University of Gävle, 801 76 Gävle, Sweden
Full list of author information is available at the end of the article

inclusions were randomly oriented ellipsoidal inclusions, which result in an isotropic permittivity.

In this paper, we present measurements of the complex permittivity of wood chips of different moisture content at microwave frequencies (0.75–2.5 GHz). In particular, we present data for the anisotropy. We use an UWB radar equipment in transmission mode, a method that is suitable also for in line industrial applications and large volumes. We also use effective medium models for the complex anisotropy. To our knowledge, experimental data and effective medium modeling of the anisotropy of the complex permittivity of wood chips vs moisture content have not been reported before.

Materials and methods

Wood chips

We analyze wood chips made of stem wood of predominantly Norway spruce (*Picea abies*) with possible small amounts of Baltic pine (*Pinus sylvestris*) from middle Sweden, i.e., conifer or softwood. The woodchips were produced for industrial purpose and in particular as fuel in district heating. It was, therefore, not possible to evaluate the permittivity and anisotropy of the wood before the it was cut into wood chips and used in the study. Figure 1 shows wood chips of stem wood of the type investigated here, where the left image is a top view and the right a side view. The side view is blurred since it is taken through transparent plastic used in the lab, in order to have the wood chips oriented as in the radio measurements (describe below). Notice that the individual wood chips have the shape of long rods in most cases. The length is in the range 1–10 cm. The short side of the individual wood chips is 10–20% of the length. The wood chips are not randomly oriented in all directions. Instead, they are oriented in such a way that the long side is predominantly horizontal (perpendicular to gravity) [8].

Experimental equipment

During the measurements the wood chips were placed in a plastic box of the type euro container (an industrial stacking container conforming to the VDA 4500 standard [12]). Four antenna housings were placed on each side of the box for radio transmission measurement (see Fig. 2). The box had the interior size of $26.8 \times 36.8 \times 31.5$ cm^3. The antenna housings were made of steel and had the size of $14.0 \times 14.0 \times 14.0$ cm^3. Each housing included one balanced Vivaldi-antenna, which could be rotated to enable the measurement of the permittivity parallel and perpendicular to gravity (cf. [13]). The transmit and receive antennas were both in the parallel or perpendicular orientation, in the respective measurement cases. The system was used in transmission mode, i.e., the antenna on one side is transmitting a signal that propagates through the wood chips and is received by the opposite antenna.

The antennas were connected to a radar system called DiRP (digital radar processor) that is based on M-sequence technology (cf. [14]), to generate the UWB signal. The sampling frequency was 25 GHz and the signal's center frequency was 2.5 GHz in a 3.5 GHz wide band. In this frequency range the signal level after propagating through wood chips is high enough to be detectable for wood chips of both high and low moisture content. Higher frequencies would be more attenuated resulting in too low signal levels. The antenna size is practical in laboratory and industry applications. Lower frequency would require larger antennas.

A conventional cement mixer (Biltema 17-686), Fig. 3 (left), was used to mix wood chips and water to get

Fig. 1 Wood chips of stem wood used in this investigation, top view (left) and side view (right). The vertical length of each image corresponds to 30 cm. The figure shows dry wood chips. The side view was photographed through a plastic container used in the experiments to get the correct orientation of the wood chips by gravity (hence the blurry image)

Fig. 2 Sample box—with antenna housings—filled with wood chips. Also shown is the coordinate system used. The antennas (not seen) are rotated inside the metallic boxes to give horizontal or vertical E-field

wood chips of moisture content. A scale (Dini Argeo IP67/IP68) was used to measure the weight of water and wood chips, Fig. 3 (right).

Experimental procedure

To characterize the wood chips, 100 pieces of wood chips were randomly selected and the dimensions were measured using a caliper. The wood chips were also put in a box of transparent plastic without any lid and photographed (see Fig. 1 above).

The moisturization process started by placing 8975 kg of relatively dry wood chips (starting chips) in a larger conditioning box. This amount was used in the successive moistening. We use the dry based moisture content,

$$M_{\mathrm{d}} = \frac{m_{\mathrm{w}} - m_{\mathrm{d}}}{m_{\mathrm{d}}}, \tag{1}$$

where m_{w} and m_{d} is the weight of the wet and dry wood chips, respectively.

Initially, the moisture content of the starting chips was measured by taking samples (à 500 g) that were weighted before, denoted m_{w1s}, and after drying, denoted m_{d1s}. The drying was performed during 24 h in + 105 °C, which is the approved industrial drying procedure in Sweden [15]. The moisture content of the starting chips, M_{d1}, was determined using Eq. 1. The moisture content of the starting chips was $M_{\mathrm{d1}} = 2.23\%$. The dry weight, m_{d1}, of the entire amount of starting chips was determined from Eq. 1, using M_{d1} and the measured weight of the starting chips, m_{w1}.

The moisture content of the wood chips was increased in a number of steps. In each step, n, the moisture content, $M_{\mathrm{d}n}$, was determined from the measured weight, $m_{\mathrm{w}n}$, and the initial weight, m_{w1} using Eq. 1. The wood chips were the same in all steps.

The moistening process was performed by sprinkling 1 L of water on the wood chips during mixing by the cement mixer (Fig. 3a) for each moistening cycle. Altogether, 10 moistening cycles were performed. Each succeeding moistening cycle (except for the first one) was based on preceding moistened wood chips. Each moistening cycle took about 30 min and the whole moistening experiment was carried out for 8 h (one working day). In each cycle, following acts and measures were made:

1. Wood chips and water were mixed in the cement mixer (Fig. 3a). Water was sprinkled over the wood chips,
2. Wood chips were moved from the cement mixer to the conditioning box and mixed again,
3. The weight, $m_{\mathrm{w}n}$, of the wood chips in the conditioning box was measured (Fig. 3b),

Fig. 3 Cement mixer for moisturizing the wood chips (left) and weighting procedure (right)

4. Wood chips were moved from the conditioning box to the sample box and mixed again,
5. The sample box was packed by shaking the box towards the floor three times and adding more wood chips until the box was filled. Approximately half of the amount of wood chips from the conditioning box was needed to fill the sample box,
6. Radio transmission measurements with antennas in vertical and horizontal direction were performed on the sample box (Fig. 2a), and
7. The weight, m'_{wn}, of the wood chips in the sample box was measured.

The mixing in both step 1 and 2 was made to achieve a homogeneous moisture distribution in the sample box.

A conventional error analysis gives the error in the measured moisture content

$$\Delta M_{dn} = \left(\frac{M_{dn}}{m_{d1}} + \frac{1}{m_{d1}}\right)\left(\frac{2m_{d1}}{m_{ds}} + 1\right)\Delta w + \frac{\Delta w}{m_{d1}}, \tag{2}$$

where Δw is the error in the weight measuring.

Determining permittivity

We determined the complex permittivity of wood chips from transmitted radar pulses. We describe the main steps of the determination method. Details can be found elsewhere [8, 13]. We model the wave propagation using the complex refractive index, $\tilde{n}$. The real and imaginary parts of the permittivity, $\tilde{\varepsilon} = \varepsilon' + i\varepsilon''$, are related to the complex refractive index $\tilde{n} = n + i\kappa$ by

$$\varepsilon' = n^2 - \kappa^2,$$

$$\varepsilon'' = 2n\kappa, \tag{3}$$

or $\tilde{n} = \sqrt{\tilde{\varepsilon}}$. We determine $\tilde{n}$ from measured radar pulses that have propagated through the wood chips. The time delay gives the real part, n, [8]. The imaginary part, κ, is obtained from the relative damping vs. frequency [13].

In a reference measurement with air in the test box, a reference pulse, $y_0(t)$, is measured vs time, t. In a second measurement a pulse, $y_1(t)$, is measured after it has been transmitted through the wood chips.

The refractive index, n, is determined from the difference in time delay between $y_1(t)$ and $y_0(t)$. In order to make the time estimate more robust, we use a technique in which the Fourier transform of a transfer function, *h(t)* was calculated as [16]

$$H(\nu) = \frac{Y_1(\nu)Y_0^*(\nu)}{Y_0(\nu)Y_0^*(\nu) + \gamma}, \tag{4}$$

where $Y_1(\nu)$ and $Y_0(\nu)$ are the Fourier transforms of $y_1(t)$ and $y_0(t)$, respectively, ν is the frequency, and * denotes the complex conjugate; *h(t)* is obtained by taking the inverse Fourier transform of $H(\nu)$. The parameter γ is small and real valued and works as noise filtering. The time of the peak value of *h(t)* is the difference in time between $y_1(t)$ and $y_0(t)$, i.e., T_1-T_0. The refractive index is determined as [8]

$$n = \frac{c_0(T_1 - T_0)}{z} + 1. \tag{5}$$

We estimate the error in the refractive index as:

$$\Delta n = (n-1)\frac{\Delta z}{z} + \frac{c_0\Delta(T_0 - T_1)}{z}, \tag{6}$$

where z is the thickness of the box, and Δz its error; $\Delta(T_1\text{-}T_0)$ is the error in the determined time difference.

The imaginary part, κ, is determined from the damping of $y_1(t)$ relative to $y_0(t)$ as described in [13]. The ratio of the signals' Fourier transforms is analyzed,

$$\frac{|Y_1(\nu)|}{|Y_0(\nu)|} = |H(0)|\exp(-(2\pi\kappa z\nu)/c_0)\beta_0\beta_1^{-1}, \tag{7}$$

where β_0 and β_1 are functions that that take into account the effects such as finite sample size and finite distance between the antennas [13]. These coefficients have small frequency dependence. We neglect all frequency dependence in H except that from the attenuation in the wood chips, which is given by the slope $\alpha = -2\pi\kappa z/c_0$. Taking the natural logarithm of Eq. 7, we get that $\ln\left(\left|Y_1(\nu)/Y_0(\nu)\right|\right)$ depends linearly on ν with the slope $\alpha = -2\pi\kappa z/c_0$. Thus, we determine the slope, α by the least square method and then calculate $\kappa = -\alpha c_0/(2\pi z)$. We estimate the error in κ as

$$\frac{\Delta\kappa}{\kappa} = \frac{\Delta\alpha}{\alpha} + \frac{\Delta z}{z}, \tag{8}$$

where $\Delta\alpha$ is the error in the fitted coefficient of a straight line by linear regression (see e.g., [17]) and Δz is the error in the thickness of the wood chips in the test box.

The error in the permittivity is obtained from putting the errors in Eq. 8 into Eq. 3,

$$\Delta\varepsilon' = 2n\Delta n + 2k\Delta k,$$
$$\Delta\varepsilon'' = 2n\Delta k + 2k\Delta n. \tag{9}$$

To describe the anisotropy of $\tilde{\varepsilon}$, we the calculate the anisotropy ratios

$$k' = \varepsilon'_{\mathrm{hor}}/\varepsilon'_{\mathrm{ver}}, \quad k'' = \varepsilon''_{\mathrm{hor}}/\varepsilon''_{\mathrm{ver}}, \tag{10}$$

where $\varepsilon'_{\mathrm{hor}}(\varepsilon''_{\mathrm{hor}})$ is the real (imaginary) part of $\tilde{\varepsilon}$ for horizontal E-field, and $\varepsilon'_{\mathrm{ver}}(\varepsilon''_{\mathrm{ver}})$ for vertical E-field, respectively.

Effective medium theory

Effective medium models (or dielectric mixing models) are used for calculating the complex dielectric permittivity, $\tilde{\varepsilon} = \varepsilon' + i\varepsilon''$, of inhomogeneous media of different materials, in which the length scale of the inhomogeneities is small compared to the wavelength of the electromagnetic radiation [9, 10]. Effective medium models like Bruggeman and Maxwell Garnett are derived from Maxwell's equations for electromagnetic wave propagation and are quasistatic approximations. The models contain physical parameters and a comparison between modeled and experimentally determined permittivity can, hence, give insight into the physics of the inhomogeneous mixing. We use three different effective medium models that include inhomogeneities that give rise to anisotropic permittivity. All models have as input parameters the permittivity and volume fractions of the different materials (in our case air, wood and water) and the depolarization factors that model the effect of anisotropic inhomogeneities (in our case the elongation of the wood chips and the air and water in between them). We use literature values for the permittivity of wood at different moisture content in the models, together with volume fractions that we estimate from the measured masses.

The relaxations mechanism of wood with moisture is complex (see e.g., [18]). To describe the effect on the permittivity we use the concept of bounded and free water [19]. At moisture contents below the fiber saturation points the water molecules are adsorbed to the cell walls and do not interact as free water molecules with the E-field. Above the fiber saturation point, some water molecules are in the cell wall cavities or on the wood chips' surfaces and interact with the E-field as in free water. The fiber saturation point is at moisture contents of around 30% [19].

Wood chips have anisotropic permittivity. There are two physical properties that may give anisotropic effective permittivity. The first is that wood has different permittivity in different directions, or more precisely, for the E-field 1) radial (to the annual rings); 2) tangential (to the annual rings), and 3) parallel to the fiber direction or tangential to the stem [20]. The second is that the wood chips that are in the shape of plates or needles are oriented by gravity such that the effective permittivity becomes different for the E-field parallel or perpendicular to gravity [8]. We use an isotropic equivalent permittivity in the models. In [21], different methods to describe an isotropic equivalent permittivity of wood were compared. It was found that the arithmetic mean of the permittivity of the three main axes differs only by a few percent from other physically motivated methods. We therefore use the arithmetic mean in the cases when we use an isotropic permittivity of wood, i.e., $\tilde{\varepsilon}_{\mathrm{w}} = 2\varepsilon_{\parallel,w} + \varepsilon_{\perp,w}$ where $\varepsilon_{\parallel,w}$ and $\varepsilon_{\perp,w}$ are the permittivity of the wood with the E-field parallel and perpendicular to the fibers, respectively.

The first model that we use is a multiphase Bruggeman (BG-MPA) effective medium model for spheroidal inclusions [10, 22]. This model has the advantage of being symmetric in the constituents, i.e., the analytical expressions do not distinguish between a host material, like air, and a particle material, like wood. This feature is advantageous in our case, since the volume fractions of the constituents may vary with water content. The spheroidal inclusions—in contrast to spherical ones—give anisotropic effective permittivity. The BG-MPA gives an effective complex permittivity for three directions, $\tilde{\varepsilon}_{e,x}$, $\tilde{\varepsilon}_{e,y}$, and $\tilde{\varepsilon}_{e,z}$, which are obtained by solving

$$\sum_{n=1}^{N} f_n \frac{\tilde{\varepsilon}_n - \tilde{\varepsilon}_{e,j}}{\tilde{\varepsilon}_{e,j} + L_{n,j}\left(\tilde{\varepsilon}_n - \tilde{\varepsilon}_{e,j}\right)} = 0 \tag{11}$$

for $\tilde{\varepsilon}_{e,j}$ for $j = x, y, z$. In Eq. 11, N is the number of different phases or materials, f_n is the volume fraction of material n, $\tilde{\varepsilon}_n$ is the complex permittivity of material n, and $L_{n,j}$ is the depolarization factor for inclusions of material n in direction j. Notice, that $f_1 + f_2 + \ldots f_N = 1$ and that $L_{n,x} + L_{n,y} + L_{n,z} = 1$ for each n. For isotropic inclusions, $L_{n,x} + L_{n,y} + L_{n,z} = 1/3$. For infinitely long needles in the z-direction, $L_{n,x} + L_{n,y} = 0$ and $L_{n,z} = 1$. When solving Eq. 11 an equation of order N in $\tilde{\varepsilon}_{e,j}$ has to be solved and consequently multiple roots are obtained. We solve the equations analytically for $N=2$ and numerically for $N=3$. Only one root is physically correct and we use the method in [23] to select the correct one. In the modeling below we use $\tilde{\varepsilon}_1$ for the permittivity air, $\tilde{\varepsilon}_2$ for wood, and $\tilde{\varepsilon}_3$ for water, respectively.

The second model that we use is the Maxwell Garnett model for layered spheroidal inclusions (MG-LSI) [24]. It is derived for a geometry of a spheroidal with a coating in a host material. It resembles the wood particles in air with the assumption of free water on the particles' surface. It gives the effective complex permittivity [24]:

$$\begin{aligned}\tilde{\varepsilon}_{e,j} &= \tilde{\varepsilon}_1 + \frac{\tilde{\varepsilon}_1\sigma_j}{1 - L_{3,j}\sigma_j},\\ \sigma_j &= (f_2 + f_3)\left[\left(\tilde{\varepsilon}_3 - \tilde{\varepsilon}_1 + \left(\tilde{\varepsilon}_3 + L_{3,j}(\tilde{\varepsilon}_1 - \tilde{\varepsilon}_3)\right)\frac{(\tilde{\varepsilon}_2 - \tilde{\varepsilon}_3)f_2/(f_2 + f_3)}{\tilde{\varepsilon}_3 + L_{2,j}(\tilde{\varepsilon}_2 - \tilde{\varepsilon}_3)}\right)\right.\\ &\quad\left.\times\left(\left(\tilde{\varepsilon}_1 + L_{3,j}(\tilde{\varepsilon}_3 - \tilde{\varepsilon}_1) + L_{3,j}(1 - L_{3,j})(\tilde{\varepsilon}_3 - \tilde{\varepsilon}_1)\frac{(\tilde{\varepsilon}_2 - \tilde{\varepsilon}_3)f_2/(f_2 + f_3)}{\tilde{\varepsilon}_3 + L_{2,j}(\tilde{\varepsilon}_2 - \tilde{\varepsilon}_3)}\right)^{-1}\right],\end{aligned} \tag{12}$$

where $\tilde{\varepsilon}_1$ is the complex permittivity of the host material (air), $\tilde{\varepsilon}_3$ of the outer layer material (water) and $\tilde{\varepsilon}_2$ of the core material (wood). f_1, f_2, and f_3 are the volume fractions of materials 1, 2, and 3, respectively, and, as for the Bruggeman model, $f_1 + f_2 + f_3 = 1$. $L_{j,n}$ are as before the depolarization factors of material n in the direction j ($j = x$, y, or z).

The third model is an anisotropic Maxwell Garnett model for spheroidal inclusions of multiple types and multiple depolarization factors (MG-MPA) [25]. The inclusion can also have different orientation and distributions of orientation. Paz et al. [11] used the Maxwell Garnett model for sawdust with randomly oriented anisotropic particles, causing an isotropic effective permittivity. We use the model assuming that all inclusions are aligned to the coordinate system of the measurements system (which is given by the orientation of the antennas, the box and the wood chips' orientation by gravity). The effective permittivity in the *x*,*y*, and *z*-directions is given by the diagonal elements of the matrix ε_e,

$$\begin{aligned}\varepsilon_e &= \tilde{\varepsilon}_1\mathbf{I} + \frac{1}{3}\sum_{n=2}^{3}\tilde{\varepsilon}_1 f_n\left[\sum_{j=1}^{3}\eta_n(\mathbf{I} + \eta_n L_{n,j})^{-1}\right]\\ &\quad\times\left\{\mathbf{I} - \frac{1}{3}\sum_{n=2}^{3}f_n\left[\sum_{j=1}^{3}L_{n,j}\eta_n(\mathbf{I} + \eta_n L_{n,j})^{-1}\right]\right\}^{-1},\end{aligned} \tag{13}$$

where $\tilde{\varepsilon}_1$ is the permittivity of the host material (air), $\mathbf{I}$ is the identity matrix and the matrix η_n is diagonal in our case with the diagonal elements

$$\eta_{n,jj} = \frac{16 f_n(\tilde{\varepsilon}_n - \tilde{\varepsilon}_1)}{3(\tilde{\varepsilon}_1 + L_{n,j}(\tilde{\varepsilon}_n - \tilde{\varepsilon}_1))}, \tag{14}$$

and $j = 1,2,3$ corresponds to the *x*, *y*, and *z*-direction, respectively. As before, $L_{n,j}$ is the depolarization factor of material n in direction j and f_n is the volume fraction of material n.

Modeling wood chips moisture content

The effective medium models above require that the volume fractions of the different materials are known. From the experiments we get the mass of the wood chips in the sample box, m'_{w}, for different moisture contents, M_{d} (we omit the index n which refers to moistening cycle). The dry weight of the wood chips in the sample box, m'_{d}, can be calculated from M_{d} and m'_{w} using Eq. 1. The weight of the water is then $m'_{\mathrm{H_2O}} = m'_{\mathrm{w}} - m'_{\mathrm{d}}$. The volume of the sample box containing the wood chips is V_{sb}.

Below the fiber saturation point (which we take to be $M_{\mathrm{d}} = 30\%$ [19]) there is no free water and the mixture consists of air and wood. The volume fraction of wood becomes

$$f_2 = \frac{m'_{\mathrm{w}}}{\rho_{\mathrm{w}} V_{\mathrm{sb}}}, \tag{15}$$

where ρ_{w} is the density of the wood, which depends on M_{d} [26]

$$\rho_{\mathrm{w}} = \rho_{\mathrm{H_2O}} G_{\mathrm{w}}(1 + M_{\mathrm{d}}), \tag{16}$$

where G_{w} is the specific gravity of wood and $\rho_{\mathrm{H_2O}} = 1$ g cm^{-3} is the density of water. The density ρ_{w} is an average of all the wood chips, similarly to the depolarization factors $L_{n,j}$. The variation in ρ_{w} will be relatively small since all wood chips are of conifer wood.

The volume fraction of air is obtained as $f_1 = 1 - f_2$ below the fiber saturation point (i.e., we set $f_3 = 0$, in the effective medium model above, since it is the volume fraction of free water).

Above the fiber saturation point, we assume that the wood's volume fraction, f_2, is the same as at the fiber saturation point ($M_{\mathrm{d}} = 30\%$); the mass of the free water, denoted $m'_{\mathrm{H_2O,fr}}$ is calculated as $m'_{\mathrm{H_2O,fr}} = m'_{\mathrm{w}} - m'_{\mathrm{w}}(30\%)$ and the volume fraction for water becomes

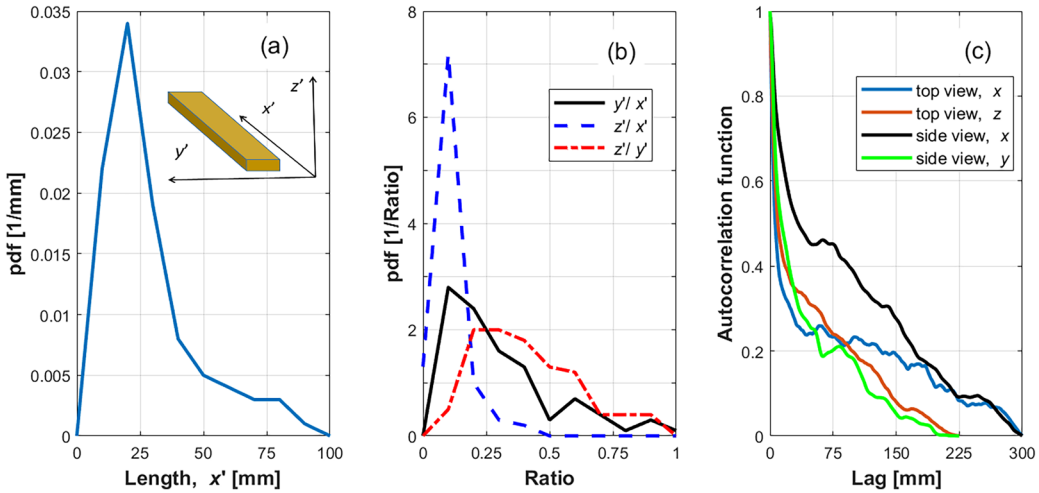

Fig. 4 **a** pdf of the wood chips' length of the longest axis, *x*'. **b** pdf of the ratios of the wood chips' lengths. **c** autocorrelation function of the images in Fig. 1 along the axis shown in Fig. 2

$$f_3 = \frac{m'_{\mathrm{H_2O}} \rho_{fr}}{\rho_{\mathrm{H_2O}} V_{\mathrm{sb}}} \tag{17}$$

and the volume fraction of air becomes $f_1 = 1 - f_2 - f_3$.

Results

Wood chips dimensions

The probability density function (pdf) of the measured dimensions of the 100 measured wood chips was calculated. The longest length is denoted *x*', the second length *y*', and the shortest *z*', as shown in the inset of Fig. 4(a). In Fig. 4(a) the pdf of the wood chips as measured along the longest axis, *x*', is shown. The length varies between 10 and 100 mm with a clear peak at 20 mm. For each wood chip the relative dimensions were calculated, and the corresponding pdf:s calculated. In Fig. 4(b) the pdf:s of the ratios *y*'/*x*', *z*'/*x*', and *z*'/*y*' are shown. The ratio *y*'/*x*' has a clear peak at 0.1, which indicates that the typical wood chip is 10 times longer than it is wide. The ratios *z*'/*x*' and *z*'/*y*' do not have that clear peaks, but it is clear that the wood chips are elongated.

The two-dimensional autocorrelation of the images (converted to gray scale) in Fig. 1 were calculated. In Fig. 4c the autocorrelation is shown for the top and side views in Fig. 1. In Fig. 4c, *x*, *y* and *z* refer to the coordinate system in Fig. 2. For the top view the *x*- and *z*-directions have mainly the same autocorrelation function, which indicates random orientation of the wood chips. For the side view the autocorrelation in the *x*-direction is clearly larger than in the *y*-direction, which indicates that the wood chips' are oriented in the *x*-direction. The autocorrelation length, ξ, is the length at which the autocorrelation function is $\xi = 1/\mathrm{e} = 0.37$. For the top view

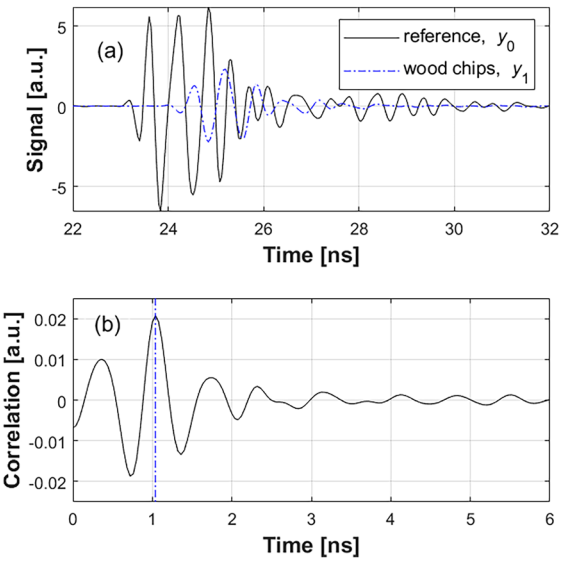

Fig. 5 **a** Example of experimental reference signal and signal that has passed wood chips signals in time domain **b** the function h(t) of the signals in **a** used to determine the time delay. The vertical line indicates the determined time delay use to obtain *n*

$\xi = 11$ mm (*x*) and $\xi = 23$ mm (*z*). For the side view $\xi = 25$ mm (*y*) and $\xi = 103$ mm (*x*). Thus, the side view shows that the wood chips are oriented in the horizontal plane.

Permittivity of wood chips vs moisture

In Fig. 5a the radar signal of a reference measurement—where the signal has passed through air—is shown with a signal that has passed through wood chips of moisture

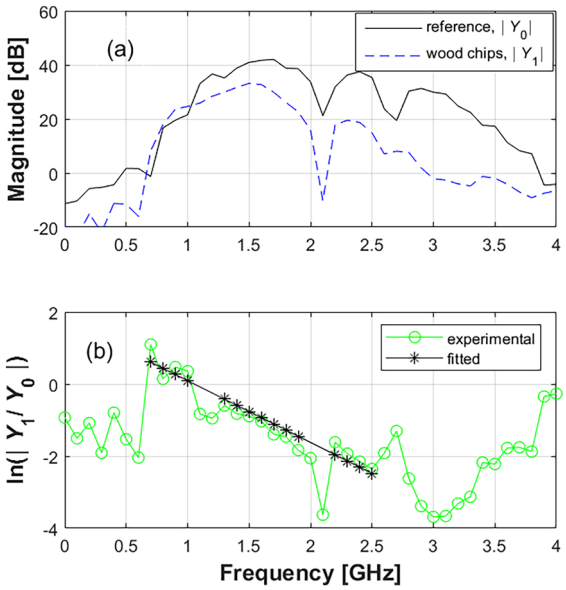

Fig. 6 **a** Amplitude vs frequency for the signal in Fig. 5 and **b** the amplitude ratio of the signals vs frequency used to determine κ

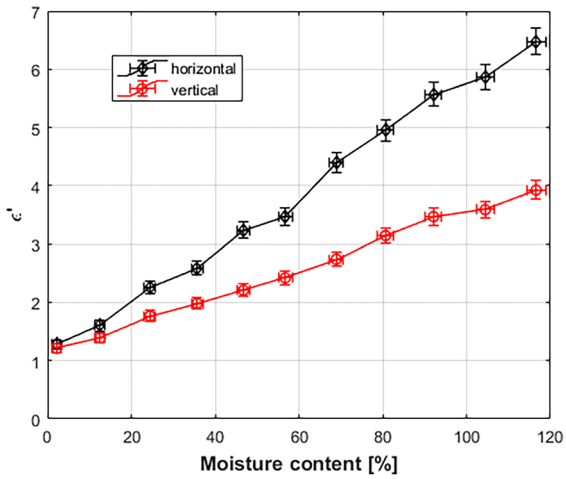

Fig. 7 The real part of the permittivity, ε', vs moisture content, M_d, for wood chips. Data for the E-field horizontal (x in Fig. 2) and vertical (y in Fig. 2) are shown

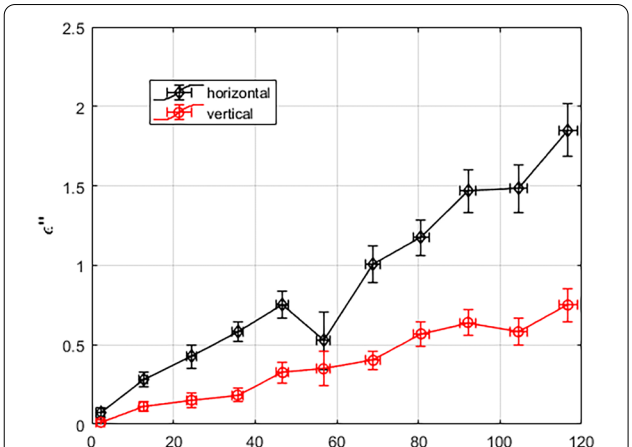

Fig. 8 The imaginary part of the permittivity, ε'', vs moisture content, M_d, for wood chips. Data for the E-field horizontal (x in Fig. 2) and vertical (y in Fig. 2) are shown

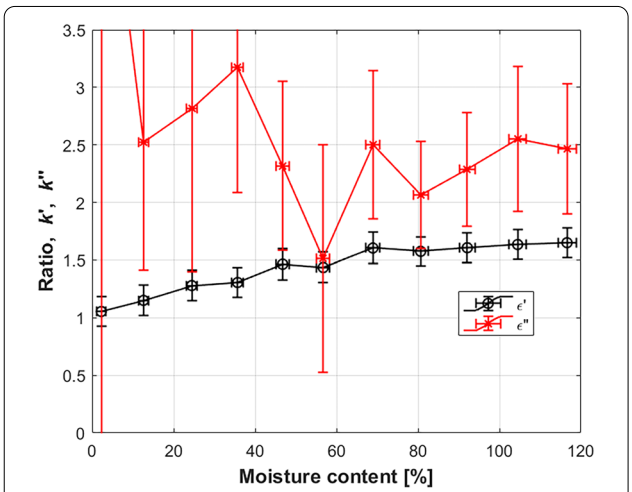

Fig. 9 Anisotropy ratios k' and k'' of the permittivity for horizontal E-field and for vertical E-field for ε', and ε'', in Figs. 7 and 8, respectively, vs moisture content, M_d

content 47%. One sees clearly that the wood chips delay the signal in time and attenuates it. In Fig. 5b the function *h(t)*, as calculated from the inverse Fourier transform of Eq. 4, is shown. The time shift is clearly seen.

To determine κ, the frequency range 0.7 to 2.5 GHz was used where the signal-to-noise ratio was high enough to enable the fitting of a straight line. In Fig. 6a the magnitude vs frequency of the two signals in Fig. 5a are shown. The signal that has passed through wood chips is clearly lower, particularly at frequencies above 2.5 GHz. In Fig. 6b the natural logarithm of the ratio of the signals in Fig. 6(a) is shown vs frequency. Also shown is the fitted straight line used to determine κ. Notice that the signals' levels are low below 0.7 GHz, at 2.1 GHz, and at 2.7 GHz where the antennas gain is low. Data points at 2.1 GHz and above 2.7 GHz were therefore not used in the determination of κ.

Figure 7 shows ε' vs M_d. It increases monotonically with M_d for both the directions of the E-field. The values for the horizontal E-field are consistently higher than those for vertical E-field.

Figure 8 shows ε'' vs M_d. It also increases monotonically (except one data point) with M_d. As for ε', the values for horizontal E-field are consistently higher than for vertical E-field.

In Fig. 9 the anisotropy ratios of the permittivity, k' and k'', are shown for the data in Figs. 7 and 8, respectively. The real part, k', increases monotonically with M_d from approximately 1.1 to 1.6. For the imaginary part, k'', the errors in the data are large. Any increase or decrease with M_d. cannot be distinguished. However, k'' is clearly larger than k' and is in the range 2 to 3 at high M_d (above 40%).

Effective medium modeling

To model the complex effective permittivity in the x-(horizontal) and y-directions (vertical), we used the models described above. We used literature values for the permittivity. The volume fractions were determined from the measured masses of the wood chips. As free parameters, used to fit the modeled permittivity to the experimental ones, we used the specific gravity, G_w in Eq. 16, and depolarization factors, $L_{n,j}$ in the respective model for $M_d < 30\%$. For $M_d > 30\%$ only the depolarization factors of free water was used as a free parameter. (The specific gravity and depolarization factors for wood and air obtained from fitting of data for $M_d < 30\%$ was used also for $M_d > 30\%$.) The modeling is described in more detail in this section.

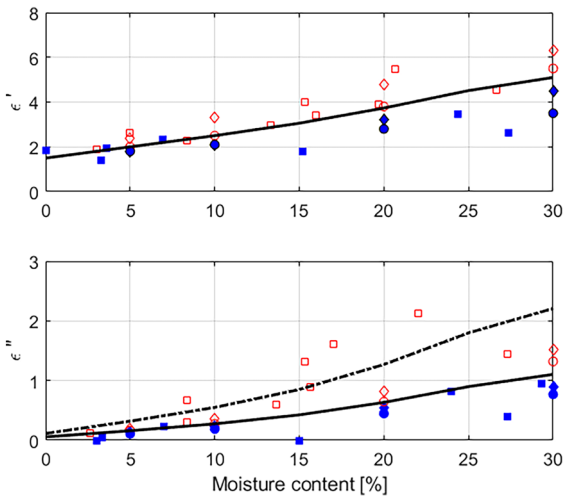

Fig. 10 Real (above) and imaginary (below) part of the permittivity of softwood vs moisture content from the literature: diamonds [26] at 0.9 GHz, circles [26] at 2.375 GHz and squares [27] at 1.26 GHz. Filled symbols for the E-field perpendicular to and open parallel to the wood fibers. The solid lines are isotropic equivalent permittivity, ε'_w and ε''_w, used in the modeling based on [26]. The dashed-dotted line is the higher value of ε''_w also used in the modeling

We use literature values for the permittivity of soft wood from ch. 5 in [27] to calculate ε_w, as described above. Figure 10 shows some literature values for the permittivity of wood vs moisture content up to 30% [27, 28]. Also shown are the values for ε_w that we use in the modeling. We see in the figure that the scattering in the data is relatively large, in particular for ε''_w. For ε'_w the values based on [27] are in the middle of given literature data. For ε''_w the values based on [27] are relatively low. We therefore also use higher values for ε''_w, also shown in the figure, to investigate the effect of the modeling results from different values of ε''_w, since the literature data show such large variations.

For the free water we use $\tilde{\varepsilon} = 79 + i5$ [29] in all the models.

Below the fiber saturation point (for $M_\mathrm{d} < 30\%$) we model $\tilde{\varepsilon}$ as a dielectric mixture of wood and air. We set $f_3 = 0$ in the BG-MPA, MG-LSI, and MG-MPA models above. The modeling is made in these steps:

a. The volume fractions of air, f_1, and wood, f_2, are calculated from the experimentally determined masses, as described above.
b. For the permittivity of wood, $\tilde{\varepsilon}_\mathrm{w}$, we used the values in Fig. 10. Thus, we use two values of ε''_w, which results in different modeled $\tilde{\varepsilon}$.
c. We use the depolarization factors, $L_{n,j}$, in the respective models to fit the modeled anisotropy ratio of ε', k', to the experimental one in Fig. 9. The anisotropy ratio of ε'', k'', has too large experimental errors to enable a fit (see Fig. 9). We set $L_{n,x} = L_{n,z} \neq L_{n,y}$ in all the models, since the wood chips are randomly oriented in the x–z-plane. In the BG-MPA model we set $L_{1,j} = L_{2,j}$ for $j = x,y$, and z. We thus reduce the number of parameters and get the more commonly used version of the model in [22].
d. We use G_w to fit the modeled ε' to the experimental one in Fig. 7. ε' is used since the experimental errors are smaller than for ε'' and the scattering in the literature data (Fig. 10) is also smaller for ε' than for ε''.

Notice, that for $M_\mathrm{d} < 30\%$ we use only two parameters in the models to fit the experimental data: The specific gravity, G_w and depolarization factor $L_{n,x}$ ($L_{n,y}$ and $L_{n,z}$ are not independent of $L_{n,x}$). The experimental values for ε'', are not used in the fit.

Above the fiber saturation point (i.e., for $M_\mathrm{d} > 30\%$) we model $\tilde{\varepsilon}$ as a mixture of air, wood and water:

i. The volume fractions of air, f_1, wood, f_2, and water, f_3, are calculated from the experimentally determined masses, as described above.

Table 1 Model parameters used in the effective medium models

Model	Depolarization factors below $M_d = 30\%$	Depolarization factors above $M_d = 30\%$	Specific gravity, G_w
BG-MPA	$L_{1,x} = L_{2,x} = L_{1,z} = L_{2,z} = 0.22$ $L_{1,y} = L_{2,y} = 1 - 2L_{1,x} = 0.56$	$L_{1,x} = L_{2,x} = L_{1,z} = L_{2,z} = 0.22$ $L_{1,y} = L_{2,y} = 1 - 2L_{1,x} = 0.56$ $L_{3,x} = L_{3,z} = 0.25$ $L_{3,y} = 1 - 2L_{3,x} = 0.5$	0.34
MG-LSI	$L_{2,x} = L_{2,z} = 0.18$ $L_{2,y} = 1 - 2L_{2,x} = 0.64$	$L_{2,x} = L_{2,z} = L_{3,x} = L_{3,z} = 0.18$ $L_{2,y} = 1 - 2L_{2,x} = 0.64$	0.33
MG-MPA	$L_{2,x} = L_{2,z} = 0.18$ $L_{2,y} = 1 - 2L_{2,x} = 0.64$	$L_{2,x} = L_{2,z} = 0.18$ $L_{2,y} = 1 - 2L_{2,x} = 0.64$ $L_{3,x} = L_{3,z} = 0.15$ $L_{3,y} = 1 - 2L_{3,x} = 0.70$	0.33

ii. For $\tilde{\varepsilon}_w$ we use the values in Fig. 10 at $M_d = 30\%$. For the free water we use $\tilde{\varepsilon} = 79 + i5$ [29].
iii. The value for G_w obtained in the modeling of data for $M_d < 30\%$ is used.
iv. For wood and air we use the depolarization factors as obtained from the modeling for $M_d < 30\%$.
v. The depolarization factors of water are used to fit the modeled anisotropy ratio, k', to the experimental in Fig. 9. We set $L_{3,x} = L_{3,z} \neq L_{3,y}$ as for $M_d < 30\%$.

Thus, we use only one free parameter, the depolarization factor of water $L_{3,x}$, as free parameters for $M_d > 30\%$ in addition to G_w and $L_{1,x}$ that were obtained from modeling for $M_d < 30\%$.

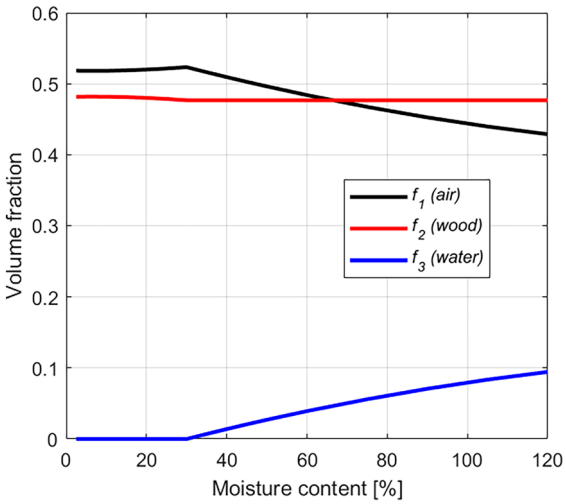

Fig. 11 Volume fraction of air, wood, and water vs moisture content for $G_w = 0.34$

Technically, the depolarization factors of air and water could be changing with moisture content, since with increasing amount of free water the geometry of the water and air inclusions may change. To vary these

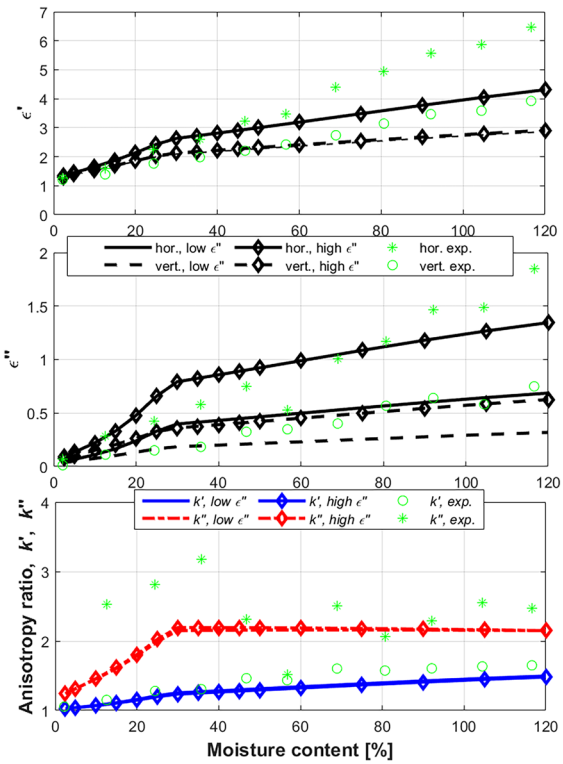

Fig. 12 Permittivity and anisotropy ratios vs moisture content, modeled using the BG-MPA model (Eq. 11) with parameters as in Fig. 10 and Table 1. For comparison the experimental data in Figs. 7, 8, and 9 are also shown

parameters with moisture content gives small improvements in the models performance.

The modeling parameters used in the different model are summarized in Table 1. In Fig. 11 the volume fractions of air, f_1, wood, f_2, and water, f_3, vs M_d, for $G_w = 0.34$, used in the BG-MPA model are shown. Up to $M_d = 30\%$ there is no free water and the volume fraction of wood is close to constant; f_2 changes marginally with M_d. Above $M_d = 30\%$ the amount of water increases and the amount of air decreases; air is replaced by water as the moisture content increases. The curve shapes of f_1, f_2, and f_3, that at not straight lines, are given by the experimental values for M_d and m'_w.

The modeled permittivity and anisotropy ratio for the BG-MPA model are shown in Fig. 12. The experimental data in Figs. 7, 8, and 9 are shown for comparison. The ratio k', increases from ca 1 to 1.3 for M_d going from 0 to 30%. This behavior is in good agreement with the experimental data in Fig. 9. The ratio, k'', increases from 1.2 to 2.2, but the experimental errors in Fig. 9 make a comparison impossible. For ε' the modeled data in Fig. 12 are in good agreement with experimental data in Fig. 7. It increases from ca 1.2 to 1.8 and 2.3 for vertical and horizontal E-fields, respectively. Notice that the modeled ε' is not significantly affected by the ε''_w used in the model. The high and low ε''_w give the same modeled ε'. For ε'', the modeled data in Fig. 12 are significantly different for the high and low ε''_w in Fig. 10. For both cases the modeled ε'' increases monotonically with M_d. The ε'' values in Fig. 12 for high ε''_w are too high by up to 30%; The ε'' values for low ε''_w are too low by up to 30%, compared with experimental data in Fig. 8. Considering the errors in Fig. 8 the modeled data for ε'' are in fair to good agreement when using the high ε''_w in Fig. 10.

For $M_d > 30\%$ the modeled anisotropy ratio k', in Fig. 12 increases to 1.5 at $M_d = 120\%$ in agreement with Fig. 9. The anisotropy ratio, k'', is practically constant at 2.2 for all M_d, also in agreement with experimental data in Fig. 9. ε' increases up to 4.5 (horizontal) and 3.0 (vertical) at $M_d = 120\%$, in qualitative agreement with Fig. 9. For ε'' the low ε''_w in Fig. 10 gives clearly too low values for $M_d > 30\%$. For the high ε''_w in Fig. 10 the modeled ε'' in Fig. 12 increases up to 1.4 (horizontally) and 0.7 (vertically) at $M_d = 120\%$ in reasonable agreement with Fig. 8. The different ε''_w values used affect in practice only the modeled ε'' values. The modeled ε' and anisotropy ratios, k' and k'', are not significantly affected.

The used value for G_w in Table 1 is well in line with data in the literature; for spruce the specific gravity is in the range 0.33 to 0.42 and for pine 0.34 to 0.51 in [30]. The depolarization factors are naturally different from those of isotropic inhomogeneities ($L_x = L_y = L_z = 1/3$).

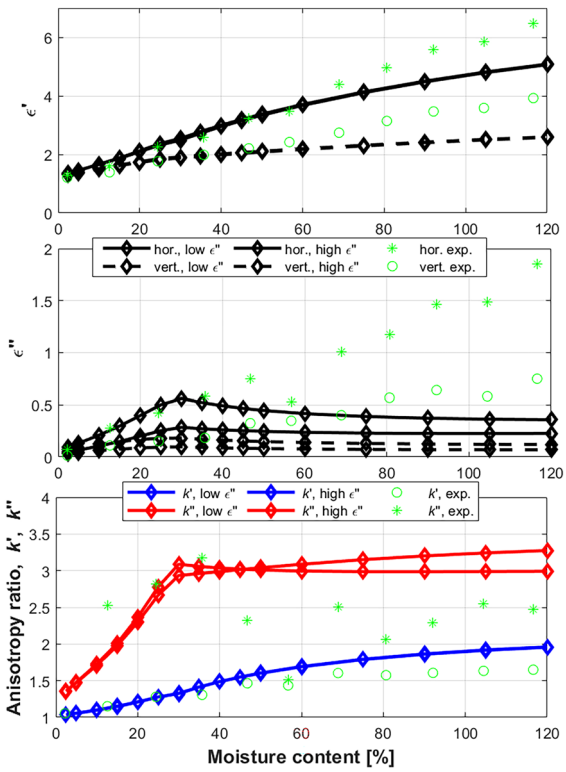

Fig. 13 Permittivity and anisotropy ratios vs moisture content, modeled using the MG_LSI model (Eq. 12) with parameters as in Fig. 10 and Table 1. For comparison the experimental data in Figs. 7, 8, and 9 are also shown

Notice that the depolarization factors for the free water ($L_{3,x}, L_{3,y}, L_{3,z}$) in Table 1 are slightly closer to a sphere than those for the wood. The explanation may be that the geometry of the water does not perfectly replicate that of the wood, but instead creates shapes that are less elongated.

Thus, using the BG-MPA model, Eq. 9, we can reproduce the main features of the experimental data in Fig. 7–9. It lends credence to the BG-MPA model, since only three free parameters were used and that the agreements is good also for ε'', which was not used in the fitting.

Figure 13 shows the model results for the MG-LSI model. For $M_d < 30\%$ the anisotropy ratios k' and k'' are similar to the BG-MPA results and are in good agreement with experimental data in Fig. 9 and 7, respectively. The modeled ε' in Fig. 13 is also in good agreement with the experimental data in Fig. 7. For ε'' the modeled data using the low ε''_w in Fig. 10 give clearly too small values, but the using the high ε''_w the agreement with experimental data in Fig. 8 is good.

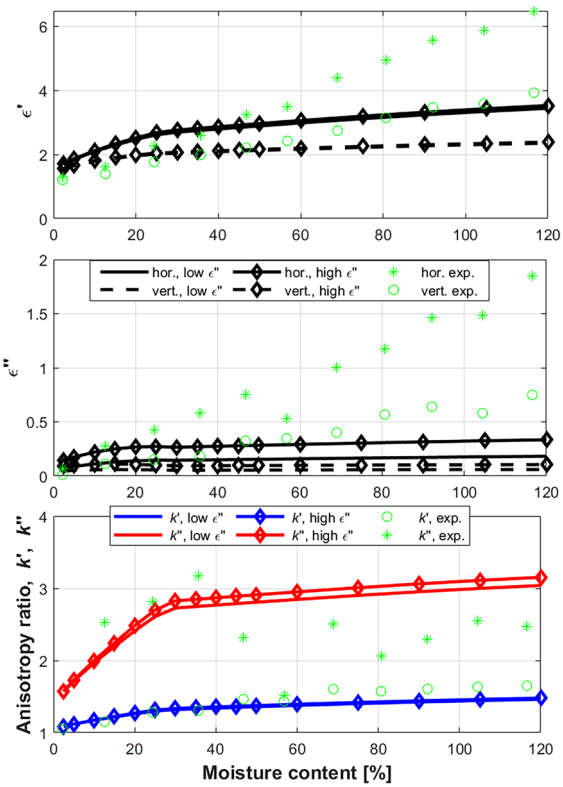

Fig. 14 Permittivity and anisotropy ratios vs moisture content, modeled using the MG_MPA model (Eq. 13) with parameters as in Fig. 10 and Table 1. For comparison the experimental data in Figs. 7, 8, and 9 are also shown

Above $M_d = 30\%$ the modeled data in Fig. 13 for the anisotropy ratios k' and k'' are too high. Notice in Table 1 that the depolarization factors for wood and free water are the same. The model was very sensitive to any difference between these depolarization factors and gave results that were in poor agreement with experiential data. ε' in Fig. 13 shows a behavior similar to the experimental data in Fig. 7. For ε'', the MG-LSI model gives values that decrease with moisture content. The results are not in agreement with the experimental data in Fig. 8. We conclude that the MG-LSI model does not well describe the complex permittivity of wood ships above the fiber saturation point. The explanation is probably that the free water does not cover the wood chips as layers of equal thickness.

The model results for the MG-MPA model are shown in Fig. 14. Up to $M_d = 30\%$ the results resemble those of the MG-LSI and BG-MPA models, both for the anisotropy ratios k' and k'', and for ε'. For ε'', however, the results are lower than for the other models and clearly lower than the experimental values, also for the high ε''_w values in Fig. 10.

For $M_d > 30\%$ the results for the MG-MPA model are in better agreement with experimental results for the anisotropy ratios in Fig. 9 than the MG-LSI model and similar to the BG-MPA model (Fig. 12). For ε' and ε'' the model gives too low values compared to the experimental ones in Figs. 7 and 8. ε'' does not change with M_d, which is slightly better in agreement with experimental results than the MG-LSI model.

Thus, the MG-LSI and MG-MPA models give reasonable results for data below $M_d = 30\%$, but become increasingly poorer with increasing moisture content. The explanation is that these models assume that the material consists of inclusions in a host material (here air), and that this assumption becomes increasingly poorer as the volume fraction of air decreases (cf. Figure 10).

Discussion

We notice that the experimental ε' and ε'' increase monotonically with moisture content for horizontal and vertical E-field. The experimental data do not show any change in behavior at $M_d = 30\%$, in contrast to all the models. The explanation is likely that the limit $M_d > 30\%$ for free water to appear is not exactly the same for all wood particles (cf. [26]) and that the moisture may not be perfectly homogeneously distributed within the wood chips, though care was taken to get homogeneous moisture distribution.

Experimental data for the permittivity of saw dust in the range 0.5 to 15 GHz increased monotonically with moisture content at all frequencies [7]; the data at 1 GHz are $\tilde{\varepsilon} = 1.5 + i0.08$ at $M_d = 15\%$, $\tilde{\varepsilon} = 2.8 + i0.28$ at $M_d = 41\%$ and $\tilde{\varepsilon} = 5 + i0.5$ at $M_d = 82\%$. They report isotropic permittivity. The data are approximately the same as our vertical ε' and our horizontal ε'' (cf. Figure 7 and 8). Notice that the size of the wood particles in [7] were around 1 mm, i.e., significantly smaller than in our case.

MG-LSI is poor above the fiber saturation point in particular compared to BG-MPA. We suggest that the explanation is that the free water does not follow the shape of layers on the wood chip surfaces. Instead it is less uniformly distributed, which explains why the MG-MPA and in particular BG-MPA are good in agreements with the experimental data.

We notice that in Ref [11] the Maxwell Garnett model was found to model the experimental $\tilde{\varepsilon}$ of woody biomass well (The biomass was mixtures of air, wood and bark). The moisture content was not as high as in our case so their results are in agreement with ours, i.e., that Maxwell Garnett can be used to model $\tilde{\varepsilon}$ at low moisture content. In [11] they did not include the Bruggeman model, but models that assume that there is a host material (air) in which the inhomogeneities are located.

Our experiments combined moistening of wood chips with radio measurements; the experimental procedure had

to be feasible for both types of experiments. The experimental time, 8 h, is shorter than, e.g., the 24 h reported in [31] for conditioning of wood chips. The individual wood chips may not have reached a homogeneous moisture distribution, which may explain some of the discrepancy between modeled and experimental permittivity. We studied industrial wood chips and in industrial applications the moistening process is not well controlled, which may affect industrial radio applications such as [8]. To our knowledge the change in permittivity with time during moistening of wood chips has not been investigated and may be the subject of future research.

Conclusions

The complex permittivity, $\tilde{\varepsilon}$, at room temperature for horizontal and vertical E-field at frequencies 0.75–2.5 GHz have been measured for wood chips vs moisture content using UWB radio technique. The elongation of the wood chips and their orientation because of gravity makes the complex permittivity anisotropic. The real part, ε', and imaginary part, ε'', increase approximately linearly with moisture content for horizontal and vertical E-fields. For $M_d \approx 0\%$,$\tilde{\varepsilon} \approx 1.2 + i0.07$ for horizontal E-field and $\tilde{\varepsilon} \approx 1.2 + i0.02$ for vertical. At the fiber saturation point, $M_d = 30\%$, $\tilde{\varepsilon} \approx 2.5 + i0.5$ for horizontal and $\tilde{\varepsilon} \approx 1.9 + i0.2$ for vertical E-field, respectively. For $M_d = 120\%$,

$\tilde{\varepsilon} \approx 6.5 + i1.8$ for horizontal and $\tilde{\varepsilon} \approx 4.8 + i0.8$ for vertical E-field, respectively.

The anisotropy ratio for ε', k', increases from 1.1 To 1.6 with moisture content going from 0 to 120%. The anisotropy ratio for ε'', k'' is significantly larger than k', in the range 2 to 3.

Three effective medium models were used to model $\tilde{\varepsilon}$ vs M_d, the BG-MPA, MG-LSI, and MG-MPA models; the number of free parameters were kept to a minimum. The volume fractions were derived from experimental data and literature values of the constituents' permittivities were used. Up to the fiber saturation point the specific gravity and the depolarization factors were used to fit experimental data; above the fiber saturation point, only the depolarization factor of the free water was used to fit the modeled to experimental data. The modeled data were fitted to ε' and k' and the model agreement for ε'' and k'' was used for model validation only.

The BG-MPA and the MG-LSI and MG-MPA models do all model the permittivity vs moisture content up to the fiber saturation point. Above that only the BG-MPA model gives results in good to fair agreement with experiments for ε', ε'', k', and k''. The better performance of the BG-MPA models has two explanations: (i) the BG-MPA model is not based on particles in a host medium, like the MG-LSI and MG-MPA models, but is symmetric in the different constituents' volume fractions, which better agrees with the structure of the wood chips. (ii) The geometry of the free water inclusions does not replicate the wood particles geometry.

In all models the modeled ε' is hardly affected by the used values for ε''_w, and in the same way, the used values for ε'_w do hardly affect the modeled ε''. The experimental errors in ε'' are relatively large and the used ε''_w are also more uncertain. The modeled anisotropy ratios depend on the polarization factors and the influence from the other model parameters is small.

Abbreviations

a: Slope of radio waves attenuation vs frequency; BG-MPA: Bruggeman-multiphase anisotropic effective medium model; $\beta 0$, $\beta 1$: Functions for the effect of finite sample size and distances; c_0: Speed of light in vacuum; E-field: Electric field; $\tilde{\varepsilon} = \varepsilon' + i\varepsilon''$: Complex permittivity; f_1, f_2, f_3: Volume fractions of air, wood chips and water; G_w: Specific gravity of wood; γ: Parameter for noise filtering of transfer function; $h(t)$, $H(\nu)$: Transfer function and it Fourier transform; k', k'': Anisotropy ratio for real and imaginary part of permittivity; $L_{n,x}$, $L_{n,y}$, $L_{n,z}$: Depolarization factors of constituent n for x, y, and z directions; MG-LSI: Maxwell Garnett-layered spherical inclusion effective medium model; MG-MPA: Maxwell Garnett-multiphase anisotropic effective medium model.; M_d, M_{dn}: Moisture content (of experimental cycle n); m_w, m_d, m_{H_2O}: Weight of wood chips, dry wood chips and free water. Index n denotes experimental cycle, m'_w, etc., means weight in sample box; m_{w1s} m_{d1s}: Weight of wet and dry wood chips used in initial moisture content determination; N: Number of phases in effective medium models; $\tilde{n} = n + i\kappa$: Complex refractive index; Pdf: Probability density function; ρ_w, ρ_{H_2O}: Density of wood and water; T_0, T_1: Travel time of radio pulse in air and wood chips; UWB: Ultra wideband; V_{sb}: Volume of sample box; $y_0(t)$, $y_1(t)$, $Y_1(\nu)$, $Y_0(\nu)$: Measured radio pulses for air and wood chips vs time t, and their Fourier transforms vs frequency ν; z: Thickness of box with wood chips.

Acknowledgements

Gävle energy is acknowledge for providing wood chips in an industrial application.

Authors' contributions

DA planned in part and performed the experiments and part of the data analysis. DR did part of the data analysis, the modeling and the writing. PO did part of the planning of the experiments and part of the writing.

Funding

Open access funding provided by University of Gävle. The research was funded by Energimyndigheten (Swedish Energy Agency).

Availability of data and materials

The datasets used and analyzed during the current study are available from the corresponding author upon reasonable request.

Declarations

Competing interests

DA and PO are with Radarbolaget, the instrument manufacturer.

Author details

[1]Department of Electrical Engineering, Mathematics and Science, University of Gävle, 801 76 Gävle, Sweden. [2]Radarbolaget AB, Box 975, 801 33 Gävle, Sweden.

Received: 11 November 2021 Accepted: 8 March 2022
Published: 14 April 2022

References

1. Černý D, Malaťák J, Bradna J (2016) Influence of biofuel moisture content on combustion and emission characteristics of stove. Agron Res 14:725–732
2. Schön C, Kuptz D, Mack R, Zelinski V, Loewen A, Hartmann H (2019) Influence of wood chip quality on emission behaviour in small-scale wood chip boilers. Biomass Convers Biorefinery 9:71–82
3. Pietilä J, Yli-Korpela A, Timonen O, Ikonen E (2015) Monitoring and control of chip quality in chemical pulping. Nord Pulp Pap Res J 30:149–159
4. Wästerlund I, Nilsson P, Gref R (2017) Influence of storage on properties of wood chip material. J For Sci 63:182–191
5. Nyström J, Dahlquist E (2004) Methods for determination of moisture content in woodchips for power plants—a review. Fuel 83:773–779
6. Samuelsson R, Burvall J, Jirjis R (2006) Comparison of different methods for the determination of moisture content in biomass. Biomass Bioenerg 30:929–934
7. Paz AM, Trabelsi S, Nelson SO, Thorin E (2011) Measurement of the dielectric properties of sawdust between 0.5 and 15 GHz. IEEE Trans Instrum Meas 60:3384–3390
8. Ottosson P, Andersson D, Rönnow D (2018) UWB radio measurement and time-domain analysis of anisotropy in wood chips. IEEE Sens J 18:9112–9119
9. Sihvola A (2000) Mixing rules with complex dielectric coefficients. Subsurf Sens Technol Appl 1:393–415
10. Markel V (2016) Introduction to the Maxwell Garnett approximation: tutorial. J Opt Soc Am A 33(7):1244–1256
11. Paz A, Thorin E, Topp C (2011) Dielectric mixing models for water content determination in woody biomass. Wood Sci Technol 45:249–259
12. "VDA Recommendation 4500: Small Load Carrier (KLT) System", Verband der Automobilindustri, 2018. http://www.vda.de. Accessed 22 Feb 2022.
13. Choudhary V, Rönnow D (2020) A nondestructive testing method for the determination of the complex refractive index using ultra wideband radar in industrial applications. Sensors 20:3161
14. Sachs J (2003) M-sequence ultra-wideband-radar: state of development and applications. In: Proceedings of the international conference on radar, Adelaide, SA, Australia, 2003
15. "Mätningsinstruktion för bestämning av torrhalt och energiinnehåll på skogsråvara (in Swedish)," Biometria 2017. http://www.sdc.se. Accessed 21 Oct 2021.
16. Al-Oudatallah J, Abboud F, Khoury M, Ibrahim H (2017) Overlapping signal separation method using superresolution technique based on experimental echo shape. Adv Acoust Vib 2017:7132038
17. Nordling C, Österman J (2020) Physics handbook. Studentlitteratur, Lund
18. Gezici-Koc Ö, Erich SJF, Huinink PH, van der Ven LGJ, Adan OCG, (2017) Bound and free water distribution in wood during water uptake and drying as measured by 1D magnetic resonance imaging. Cellulose 24:535–553
19. Berry SL, Roderick ML (2005) Plant–water relations and the fibre saturation point. New Phytol 168:25–37
20. Fediuk A, Wilken D, Wunderlich T, Rabbel W (2020) Physical Parameters and contrasts of wooden objects in lacustrine environment: ground penetrating radar and geoelectrics. Geosciences 10:146
21. Olmi R, Bini M, Ignesti A, Riminesi C (2000) Dielectric properties of wood from 2 to 3 GHz. J Microw Power Electromagn Energy 35:135–143
22. Schmidt D (2014) Characterization of highly anisotropic three-dimensionally nanostructured surfaces. Thin Solid Films 571:364–370
23. Jansson R, Arwin H (1994) Selection of the physically correct solution in the n-media Bruggeman effective medium approximation. Optics Commun 106:133–138
24. Jones SB, Friedman SP (2000) Particle shape effects on the effective permittivity of anisotropic or isotropic media consisting of aligned or randomly oriented ellipsoidal particles. Water Resour Res 36:2821–2822
25. Koledintseva MY, DuBroff RE, Schwartz RW (2009) Maxwell Garnett rule for dielectric mixtures with statistically distributed orientation of inclusions. Progress Electromagn Res 99:131–148
26. Glass SV, Zelinka SL (2010) Moisture relations and physical properties of wood. in: wood handbook-wood as an engineering material. Forest products laboratory, general technical report FPL-GTR-190. Department of Agriculture, Madison, WI, ch. 4.
27. Torgovnikov GI (1993) Dielectric properties of wood and wood-based materials. Springer, Berlin
28. Razafindratsima S, Sbartaı ZM, Demontoux F (2017) Permittivity measurement of wood material over a wide range of moisture content. Wood Sci Technol 51:1421–1431
29. Ellison WJ, Lamkaouchi K, Moreau JM (1996) Water: a dielectric reference. J Mol Liq 68:171–279
30. Kretschmann DE (2010) Mechanical properties of wood. in: wood handbook-wood as an engineering material. Forest products laboratory, general technical report FPL-GTR-190. Department of Agriculture, Madison, WI, ch. 5.
31. Hofmann N, Borchert H (2022) Influence of fuel quality and storage conditions on oxygen consumption in two different wood chip assortments—determination of the storage-stable moisture content. Fuel 309:122196

Publisher's Note